Efficient Method to Predict Noise Radiated from Rotating Sources and Scattered by an Axisymmetric Body

Yijun Mao[1*], Zhiwei Hu[2†], Yuanyuan Gu[1‡]

1 Xi'an Jiaotong University, 710049 Xi'an, People's Republic of China

2 University of Southampton, SO17 1BJ Southampton, United Kingdom

This paper presents an efficient method for predicting noise radiated from rotating sources and scattered by an axisymmetric body, where a frequency-domain numerical method and a null-field method are employed to compute acoustic radiation and scattering phenomena, respectively. The novelty of the present research is that an advanced method is proposed to locate fictitious interior observers inside the scattering surface, contributing to that the incident acoustic pressure received by the fictitious interior observers can be efficiently computed. Numerical cases show that the developed method ensures high computational accuracy and significantly improves the computational efficiency compared with existing methods, showing an appealing application potential in efficiently predicting rotor noise scattered by the shaft and casing. Parametric studies are carried out to investigate effects of the hub-tip ratio and the rotating frequency on a rotor noise scattered by a hub.

Nomenclature

c_0	=	speed of sound in fluid, m s^{-1}
C	=	solid angle coefficient
e	=	unit vector of the coordinate system
f	=	data surface function

[*]Associate professor, Department of Fluid Machinery and Engineering, School of Energy and Power Engineering; maoyijun@mail.xjtu.edu.cn. Member AIAA.

[†] Lecturer, Aerodynamics and Flight Mechanics Research Group, Faculty of Engineering and the Environment. z.hu@soton.ac.uk. Member AIAA.

[‡] Ph.D. Student, Department of Fluid Machinery and Engineering, School of Energy and Power Engineering.

f_r = source rotational frequency, Hz

f_0 = source pulsating frequency, Hz

G = frequency-domain Green's function

H = Heaviside function

k = wavenumber, ω/c_0 , m^{-1}

$\mathbf{L}$ = time-domain strength of loading source, Pa

L_M = $L_i M_i$, Pa

L_r = $L_i \hat{r}_i$, Pa

$\dot{L}_r$ = $\frac{\partial L_i}{\partial \tau} \hat{r}_i$, Pa s^{-1}

m = harmonic number

n_i = components of unit vector normal to the data surface

$\tilde{p}'$ = acoustic pressure in frequency domain, Pa

Q = time-domain strength of thickness source, kg m^{-2} s^{-1}

$\tilde{Q}_E$ = frequency-domain strength of the equivalent monopole source for the ESM, kg s^{-1}

$\tilde{Q}_S$ = frequency-domain strength of the equivalent dipole source for the NFM, N

r = geometrical distance between the source and the receiver, $|\mathbf{x}-\mathbf{y}|$, m

r_i = components of the vector in the radiation direction, $x_i - y_i$,m

r_t = radius of the blade tip, m

r_h = radius of hub, m

$\hat{r}_i$ = components of the unit vector in the radiation direction, r_i/r

T_{int} = interval length of time-domain integral, s

t = observer time, s

$\tilde{\mathbf{u}}'$ = frequency-domain acoustic velocity, m s^{-1}

u_i = components of the fluid velocity, m s^{-1}

u_n = local normal component of the fluid velocity, m s^{-1}

v_n = local normal component of the data surface velocity, m s^{-1}

$\mathbf{x}$ = observer position vector, m

x_i = components of the observer position vector, m

$\mathbf{y}$ = source position vector, m

y_i = components of source position vector, m

β = normalized surface admittance

ϕ = azimuth angle, rad

θ = elevation angle, rad

ρ = local fluid density, kg m^{-3}

ρ_0 = fluid density of unperturbed medium, kg m^{-3}

ρ' = density perturbation, kg m^{-3}

$\delta(\cdot)$ = Dirac delta function

σ_{ij} = components of viscous stress tensor, Pa

τ = source time, s

Γ = scattering surface

ω = angular frequency, rad s^{-1}

ω_0 = angular frequency of source pulsation, rad s^{-1}

ω_r = angular frequency of source rotation, rad s^{-1}

Subscripts

0 = fluid variable for the unperturbed medium

I = incident component

L = loading source

T = thickness source

x = observer quantity

y = source quantity

I. Introduction

OVER the past several decades, noise radiated from rotors and scattered by solid surfaces has been an important topic of research on turobomachinery and aircraft noise, and developing accurate and efficient numerical methods is beneficial for understanding the noise radiation and propagation mechanism and for controlling noise level by optimizing the acoustic liner design.

Among various numerical prediction methods, finite element method (FEM) and boundary element method (BEM) are very popular in solving acoustic radiation and scattering problems. Generally, the BEM has several advantages over the FEM. Firstly, the entire acoustic domain needs to be discretized for the FEM, thus limiting its ability to predict the far-field noise, while the BEM only discretizes solid surfaces and performs surface integrals, making it easily applicable for observers at an arbitrary position. Secondly, the Sommerfeld radiation condition is naturally satisfied in the BEM, while the FEM requires extra treatments on the domain boundary, such as non-reflecting boundary conditions [1], perfectly matched layer [2] and using infinite elements [3], to avoid any spurious reflection of sound waves from artificial boundaries, and to satisfy the free-field condition. Thirdly, the FEM subjects to dispersion and dissipation errors, which do not appear in the BEM. However, the FEM has an advantage over the BEM in solving sound propagation in non-uniform flow. Detailed comparison and analysis on the above two methods can be found in reference [4].

Moreover, solutions of the BEM usually suffer from a non-uniqueness problem at irregular frequencies which must be treated carefully. Two typical techniques, namely the combined Helmholtz integration equation formulation (CHIEF) proposed by Schenck [5] and the Burton-Miller method [6], are usually applied to deal with the non-uniqueness. In the Burton-Miller BEM, strongly singular and hyper-singular integrals arising from the normal derivative of the integral equation would cause substantial difficulties in computational operations. Many studies have been conducted to resolve this issue. Early studies started from Burton and Miller [6], who used a double surface integral method to reduce the order of singularity. The double surface method is restricted due to its high computational cost, and some methods on regularizing the hyper-singular integrals have been carried out, see for examples [7, 8], but the increased computational time remains a limiting factor for the BEM.

An efficient way to deal with the singularity problem is to use the equivalent source method (ESM) [9-11]. A crucial step for the ESM is to construct equivalent sources inside the scattering surface to satisfy the desired acoustic

boundary condition on the scattering surface. Since the observers are confined on the scattering surface and are therefore kept a certain distance from the equivalent sources, the singularity problem is automatically eliminated. The acoustic boundary condition on the scattering surface, i.e. the linear relation between the acoustic pressure and the acoustic pressure gradient or acoustic velocity, is usually used to determine the equivalent source strengths inside the scattering surfaces for the ESM. Recently, Ghorbaniasl et al. [12] and Mao et al. [13] have developed analytical time-domain and frequency-domain acoustic velocity formulations which are mathematically simpler than the analytical acoustic pressure gradient formulation [14]. Since the acoustic velocity and acoustic intensity are vectors, the method of directly computing these vectors is named vector acoustics method (VAM) [15]. Mao et al. [16, 17] have combined the ESM with the VAM to visualize the propagation of acoustic energy radiated from sources and scattered by solid surfaces and to directly compute the acoustic power absorbed by the impedance scattering surface.

The acoustic scattering phenomenon can also be studied by using the null-field method (NFM). The basic idea of the NFM is to determine the source strength on the scattering surface by fixing some fictitious observers (field points) inside the scattering surface. This treatment is similar to the ideas of the BEM and the ESM but has a subtle difference. Both the equivalent sources and the observers are located on the scattering surface in the BEM which causes singularity, while in the ESM the equivalent sources and the observers are, respectively, located ***inside and on*** the scattering surface which avoids singularity. In the NFM, the equivalent sources and the fictitious observers are located ***on and inside*** the scattering surface, respectively, thus the NFM is also able to avoid singularity. The idea of the NFM was firstly proposed by Waterman to compute the electromagnetic [18] and acoustic [19] scattering in 1960s, which was almost at the same time that the FEM and the BEM were developed. The NFM, which is also called T-matrix method, has been commonly used for light and electromagnetic scattering from small particles [20]. Cunefare et al. [21] has employed the idea of the NFM to numerically compute acoustic radiation from a vibrating surface. Moreover, Martin [22, 23] has presented a rigorous mathematic proof and showed that the NFM can always avoid the non-uniqueness problem in two-dimensional space, and he also conjectured that this conclusion would be true in three dimensions.

With no singularity, the ESM and the NFM are usually simpler and computationally more efficient than the BEM. Moreover, another advantage of the ESM over the BEM is that the number of interior equivalent sources can be less than that of scattering surface elements [9], which makes the ESM more efficient owing to the reduced size of the linear equation system. It has been shown that the ESM can achieve a good computational accuracy with equivalent

sources only half of the scattering surface elements [10, 11], which would greatly reduce the calculation needed. In both the BEM and the ESM, it is an essential step to compute the acoustic pressure gradient or the acoustic velocity at observers located on the scattering surface. However, only the acoustic pressure received by the observers is needed in the NFM, thus the NFM can further improve the computational efficiency for acoustic scattering. Discussions and illustrations will be presented in more details in Setion III.

There are three time-consuming modules in the BEM, ESM and NFM. The coefficient matrixes for all three methods are full rank, and they are time-consuming to construct and solve, especially for a large number of surface elements producing a high-order coefficient matrix. For practical problems, parallel computation is normally needed and the fast multipole method (FMM) [24] can help to speed up the calculation, but the FMM is not suitable for noise radiated from rotating sources. Besides constructing the coefficient matrix and solving the linear equation system, another time-consuming module for these methods is the numerical integral required to calculate noise radiated from sources and received by observers on the scattering surface. If we assume that the numbers of on distributed sources and scattering surface elements are N_I and N_S, respectively, N_I*N_S numerical integrals will be required to calculate the noise radiated from the distributed sources. In the case of rotating sources, predicting the incident sound costs even more than constructing the coefficient matrix and solving the linear equation system. Based on the above analysis, it is of practical importance to accelerate the computation of the rotor noise scattering.

This paper aims to develop an efficient method for predicting noise radiated from rotating sources and scattered by an axisymmetric body, such as the centerbody of open rotors [25, 26], the shaft and the casing of axial tubomachinery [27, 28]. The ESM has been previously combined with the VAM to compute sound scattered by impedance surfaces [16]. Furthermore, a frequency-domain numerical method for predicting the rotor noise scattered by solid surfaces has been validated [17], where the frequency-domain acoustic pressure [29] and acoustic velocity [13] formulations are employed to predict noise radiated from rotating thickness and loading sources. Moreover, an efficient method has been recently developed to accelerate the computation of the acoustic far field around rotating sources [30]. This paper employs the frequency-domain numerical method to compute noise radiated from rotating sources and the NFM to predict noise scattered by an axisymmetric body. Compared with the BEM and ESM used in the previous studies, the NFM used in this paper is computationally more efficient because it avoids the time-consuming step of the acoustic pressure gradient or the acoustic velocity computation. Moreover, the novelty of the present research is that an advanced method is proposed to locate the fictitious interior observers

for the NFM. With this advanced observers-location method (OLM), an efficient method, which is similar to that developed in reference [30], is used to accelerate the computation of the incident noise radiated from rotating sources. Owing to this development, the improved NFM shows a great advantage over the ESM in the computational efficiency of predicting the noise radiated from rotating sources and scattered by an axisymmetric body.

The rest of the paper is organized as follows. Section II presents the numerical methods related to predicting the noise radiated from rotating sources and scattered by surfaces, where both the ESM and the NFM are briefly reviewed and an advanced method for locating the fictitious interior observers is proposed and described in detail. In section III, four numerical test cases are carried out to validate the ESM and the NFM, moreover, the computational accuracy and efficiency are compared and discussed. Conclusions are given in Section IV.

II. Methodology

A. Numerical method for predicting incident noise radiated from rotating sources

The time-domain acoustic pressure formulation 1A proposed by Farassat [31] can be used to predict the noise radiated from the thickness and loading sources. For the noise radiated from rotating sources, the frequency-domain acoustic pressure formulation F1A developed by Tang et al. [29] is as follows

$$4\pi \tilde{p}_T'(\mathbf{x},\omega) = -\mathrm{i}\omega \int_0^{T_{\mathrm{int}}} \int_{f=0} \frac{Q}{r} w(\tau) e^{\mathrm{i}kr} e^{\mathrm{i}\omega\tau} \mathrm{d}S\mathrm{d}\tau \tag{1}$$

$$4\pi \tilde{p}_L'(\mathbf{x},\omega) = \int_0^{T_{\mathrm{int}}} \int_{f=0} \frac{L_r}{r^2}\left(1-\mathrm{i}kr\right) w(\tau) e^{\mathrm{i}kr} e^{\mathrm{i}\omega\tau} \mathrm{d}S\mathrm{d}\tau \tag{2}$$

where subscripts T and L represent the thickness and loading noise, respectively; tilde ~ means the frequency-domain component of the physical parameter; $\mathbf{x}$ and $\mathbf{y}$ represent the observer and source positions, respectively, and $r = |\mathbf{x}-\mathbf{y}|$; τ is the source time and S represents the solid surface defined by f=0; ω is the angular frequency of the noise received by observers; $k = \omega/c_0$ is the acoustic wavenumber; $w(\tau)$ is a window function; Q is the monopole source strength; L_i is the component of the dipole source strength in the ith direction; $L_r = L_i\hat{r}_i$, $\hat{r}_i = r_i/r$. Note that the Einstein notation is used in this paper, where a repeated index indicates summation over all components. By assuming that the pulsating frequency and the rotational frequency of the source are equal to f_r

and f_0, respectively, the rectangular window function $w(\tau)=1$ is usually appropriate and the interval length of integration should be $T_{\text{int}}=[1/f_r, 1/f_0]_{\text{LCM}}$, where $[]_{\text{LCM}}$ represents the least common multiple [29]. In the NFM, Eqs. (1) and (2) are employed to compute the incident acoustic pressure received by the fictitious observers inside the scattering surface.

Following the time-domain acoustic velocity formulation V1A of Ghorbaniasl et al. [12], Mao et al. [13] proposed the following the frequency-domain acoustic velocity formulation FV1A

$$4\pi\rho_0\tilde{u}'_{Ti}(\mathbf{x},\omega)=\int_0^{T_{\text{int}}}\int_{f=0}\frac{Q\hat{r}_i(1-\mathrm{i}kr)}{r^2}w(\tau)e^{\mathrm{i}kr}e^{\mathrm{i}\omega\tau}dSd\tau \tag{3}$$

$$4\pi\rho_0c_0\tilde{u}'_{Li}(\mathbf{x},\omega)=-\int_0^{T_{\text{int}}}\int_{f=0}\left(\frac{\mathrm{i}kL_r\hat{r}_i}{r}+\frac{L_i-3L_r\hat{r}_i}{r^2}+\frac{\mathrm{i}(L_i-3L_r\hat{r}_i)}{kr^3}\right)w(\tau)e^{\mathrm{i}kr}e^{\mathrm{i}\omega\tau}dSd\tau \tag{4}$$

where subscript i represents the ith direction; c_0 is the sound speed of the unperturbed medium. The numerical integration and validation of formulations F1A and FV1A can be found in references [13, 29].

In this paper, formulations F1A and FV1A are respectively employed to compute the incident acoustic pressure and acoustic velocity radiated from the rotating sources owing to the following reasons. Firstly, compared with the time-domain formulations 1A and V1A, formulations F1A and FV1A directly output the frequency-domain acoustic pressure and acoustic velocity, respectively, providing a convenient data input to predict noise scattered by the surface. Secondly, the acceleration method presented in Section II.C is only suitable for calculating the frequency-domain acoustic parameters. Moreover, the acoustic velocity is usually more time-consuming to compute than the acoustic pressure because formulation FV1A is mathematically more complicated than formulation F1A, as shown in Eqs. (1)-(4).

B. Numerical methods for acoustic scattering

As reviewed in Section I, both the ESM and the NFM avoid the singularity and non-uniqueness problems, thus have advantages over the Burton-Miller BEM in the computational efficiency. Therefore, we only focus on the ESM and the NFM for predicting the noise scattered by surfaces in the present paper. The main ideas and computational steps of these two methods are described briefly below.

The boundary integral equation describing sound radiated from sources and scattered by a solid surface $\Gamma=0$ is given by

$$C(\Gamma)\,\tilde{p}'(\mathbf{x},\omega)=\tilde{p}'_I(\mathbf{x},\omega)+\int_{\Gamma=0}\frac{\partial\tilde{p}'(\mathbf{y},\omega)}{\partial\mathbf{n}(\mathbf{y})}G(\mathbf{x},\mathbf{y},\omega)\,d\Gamma-\int_{\Gamma=0}\tilde{p}'(\mathbf{y},\omega)\frac{\partial G(\mathbf{x},\mathbf{y},\omega)}{\partial\mathbf{n}(\mathbf{y})}d\Gamma \tag{5}$$

and the boundary condition on the impedance scattering surface is

$$\beta(\tilde{p}'_I+\tilde{p}'_S)+\rho_0c_0(\tilde{u}'_{In}+\tilde{u}'_{Sn})=0 \tag{6}$$

where $\mathbf{n}(\mathbf{y})$ is the unit outward normal to the scattering surface; β is the normalized surface admittance; $\tilde{p}'_I(\mathbf{x},\omega)$ is the incident acoustic pressure; $\tilde{u}'_{In}(\mathbf{x},\omega)$ and $\tilde{u}'_{Sn}(\mathbf{x},\omega)$ are the components of the incident and scattered acoustic velocities normal to the scattering surface, respectively; $G(\mathbf{x},\mathbf{y},\omega)$ is the Green's function in three-dimensional free space expressed as

$$G(\mathbf{x},\mathbf{y},\omega)=\frac{e^{ikr}}{4\pi r} \tag{7}$$

where $r=|\mathbf{x}-\mathbf{y}|$; $C(\Gamma)$ is the solid angle coefficient which could be computed from a complicated formula. For a smooth closed scattering surface Γ, the value of $C(\Gamma)$ is given by

$$C(\Gamma)=\begin{cases}0 & \Gamma<0\\ 1/2 & \Gamma=0\\ 1 & \Gamma>0\end{cases} \tag{8}$$

In the ESM, the equivalent point sources are fixed inside the scattering surface, and the noise scattered by the surface is equal to that radiated from the equivalent sources. The strengths of the equivalent point sources are determined by employing an appropriate acoustic boundary condition (Eq. (6)) on the scattering surface, where both the incident acoustic pressure and acoustic velocity for sound radiated from the physical sources should be computed. Although different types of the equivalent sources can be used, monopole point sources are selected in the present work because it is computationally more efficient than other types of equivalent sources [16]. There is no universal rule to locate the interior equivalent sources, generally a scaled replica of the scattering surface is suggested by some researchers [9-11] for simplicity, where a scale ratio (SR) is defined to shrink the scattering surface and to locate the equivalent sources inside the scattering surface.

In the NFM, the fictitious observers are fixed inside the scattering surface, and the method for locating the fictitious observers usually follows that used in the ESM for locating the equivalent sources, which will be described detailed in next section. Since all the observers inside the scattering surface cannot receive any sound, the incident

acoustic pressure is just opposite to the scattering acoustic pressure. By employing the above feature and the acoustic boundary condition on the scattering surface, the equivalent source strength on the scattering surface is numerically calculated.

To compute the scattering acoustic wave, both the ESM and the NFM should solve a linear equation system given in matrix form by $\mathbf{A}\boldsymbol{\xi}=\mathbf{b}$, where $\mathbf{A}$ is a coefficient matrix, vector $\mathbf{b}$ is calculated from the incident sound wave, and $\boldsymbol{\xi}$ is the unknown vector which is related to the strength of equivalent sources in the ESM and in the NFM, respectively. Table 1 presents the detailed expressions of the above-mentioned matrix and vectors, in which $\tilde{Q}_E$ is the frequency-domain complex strength of the equivalent sources ***inside*** the scattering surface for the ESM and $\tilde{Q}_S$ is the frequency-domain complex strength of the equivalent sources ***on*** the scattering surface for the NFM. This numerical process contains the following three time-consuming modules: constructing the coefficient matrix $\mathbf{A}$, formulating the vector $\mathbf{b}$ and solving the matrix to obtain the unknown vector $\boldsymbol{\xi}$.

Table 1 Coefficient matrixes and vectors in the ESM and NFM

	Coefficient matrix $\mathbf{A}$	Known vector $\mathbf{b}$	Unknown vector $\boldsymbol{\xi}$
Monopole ESM	$-\mathrm{i}\omega\beta G(\mathbf{x},\mathbf{y},\omega)+c_0\dfrac{\partial G(\mathbf{x},\mathbf{y},\omega)}{\partial\mathbf{n}(\mathbf{x})}$	$\beta\tilde{p}'_I(\mathbf{x},\omega)+\rho_0 c_0\tilde{u}'_{In}(\mathbf{x},\omega)$	$\tilde{Q}_E$
NFM	$-\mathrm{i}k\beta G(\mathbf{x},\mathbf{y},\omega)-\dfrac{\partial G(\mathbf{x},\mathbf{y},\omega)}{\partial\mathbf{n}(\mathbf{y})}$	$\tilde{p}'_I(\mathbf{x},\omega)$	$\tilde{Q}_S$

In Section III, the computational time of these modules will be compared and analysed. The result will show that, for noise radiated from rotating sources, formulating the vector is the most time-consuming module. Owing to the above reason, an efficient method is proposed in Section II.C to accelerate the computation of the incident noise radiated from rotating sources.

C. Methods for locating the fictitious interior observers

Since there is no general rule for locating the equivalent sources inside the scattering surface in the ESM, a commonly used method is to locate the equivalent sources on a small replica of the scattering surface, with a specific SR. The same method can also be used to define the location of the fictitious interior observers in the NFM for its simplicity. In this paper, this conventional method for locating the fictitious interior observers is named OLM1.

Here, we develop a new method for locating the fictitious interior observers which can significantly improve the computational efficiency for predicting noise radiated from rotating sources and received by multiple observers. In previous studies, Mao et al. [32, 33] have deduced the analytical solutions for noise radiated from the rotating monopole, dipole and quadrupole point/compact sources by employing a spherical harmonic series expansion method. The analytical solutions reveal that, for noise radiated from rotating sources, the frequency-domain acoustic pressure at two observers with only different circumferential angles is proportional to their phase difference, that is [32, 33]

$$\frac{\tilde{p}'(r_x,\phi_{x_2},\theta_x,\omega_m)}{\tilde{p}'(r_x,\phi_{x_1},\theta_x,\omega_m)}=e^{\mathrm{i}m(\phi_{x_2}-\phi_{x_1})} \tag{9}$$

with

$$k_m=\omega_m/c_0=\frac{2\pi(f_0+mf_r)}{c_0} \tag{10}$$

where $(r_x,\phi_{x_1},\theta_x)$ and $(r_x,\phi_{x_2},\theta_x)$ represent the coordinates of two observers given in spherical coordinate system; m is the harmonic number; k_m is the wavenumber. Eq. (9) implies that if the observers have the same radial coordinate r_x and elevation angle θ_x, and the acoustic pressure received by the observer $(r_x,\phi_{x_1},\theta_x)$ has been numerically computed from either Eqs. (1) or (2), the acoustic pressure received by the other observer $(r_x,\phi_{x_2},\theta_x)$ can be simply and efficiently computed without performing any numerical integral. This feature combined with other features has been used to fast compute the acoustic power output from rotating sources [30]. It should be noted this feature is only valid for calculating the frequency-domain acoustic quantities, thus the frequency-domain formulations given in Section II.A are employed to compute the incident sound in the present paper. Additionally, if we compute tonal noise radiated from rotating blades which are evenly distributed along the circumferential direction, it is reasonable to assume that the source strengths on adjacent blade surfaces only differ by a constant phase, which is similar to the expression given in Eq. (9). Therefore, it is only needed to numerically calculate tonal noise radiated from a single rotating blade, and noise radiation from other rotating blades can be fast computed by using the feature of phase delay without performing numerical integrals. Details can be found in reference [34].

By employing the above-mentioned feature of noise radiated from rotating sources, a new method for locating the fictitious interior observers named OLM2 is proposed as follows. Theoretically, all the fictitious interior observers can be located on a circle to use Eq. (9) to accelerate the computation of sound received by the fictitious

interior observers. However, this treatment may form an ill-conditioned coefficient matrix, because one drawback of the ESM and the NFM is that the coefficient matrix **A** would be ill-conditioned if the locations of the equivalent sources or the fictitious observers are inappropriate [21]. Some contributing explorations have been carried out to avoid generating an ill-conditioned matrix, see for examples [35-40]. In this paper, we do not carry out a detailed research on this topic but the ill-conditioned matrix could be avoided as long as the equivalent sources and fictitious observers are not concentrated in a small region nor too close to the scattering surface, thus we can artificially put the observers on some circles with different diameters and elevation angles, and the basic principal is to disperse the fictitious observers as much as possible to avoid a large condition number of the coefficient matrix.

We denote the numbers of the acoustically compact elements on the rotating source and the scattering surface as N_I and N_S, respectively, and the number of the equivalent sources/interior observers N_E. In the ESM, N_I*N_S operations of the numerical integrals should be performed to compute the incident acoustic velocity. For the NFM with OLM1, N_I*N_E operations should be performed to compute the incident acoustic pressure. However, the operations of the numerical integrals for the NFM with OLM2 are much less because all the fictitious observers are located on a few circles, and only N_I operations should be performed for the observers on each circle.

In Section III, both of these two methods for locating the interior observers will be tested. The numerical result will validate that the NFM combined with OLM2 not only achieves a good computational accuracy but also greatly improves the computational efficiency.

III. Numerical Cases and Discussion

A. Numerical cases

Mao et al. [17] combined the frequency-domain formulations F1A and FV1A with the ESM to predict noise radiated from rotating sources and scattered by surfaces, where three numerical cases are carried out to validate the developed numerical method. In this paper, we employ the same numerical cases as those used in reference [17], thus only a brief introduction on the numerical cases is given here. Moreover, the developed method is used to analyze noise radiated from a realistic rotor and scattered by a hub, which is shown in test case 4.

Test Case 1*: noise radiated from a rotating monopole point source and scattered by a rigid sphere.*

The monopole point source rotates counterclockwise around the Z axis at radius $r_y = 1.2$ m on the *xy* plane ($\theta_y = \pi/2$) and the initial azimuthal angle is $\phi_0 = 0$. The rotational frequency f_r of the source is 40Hz and it has a

constant source strength $\int_{f=0} QdS = 1\,\mathrm{kg}\cdot\mathrm{s}^{-1}$. The scattering sphere with a radius of $a = 1m$ is centered at the origin of the coordinate system.

***Test Case 2**: noise radiated from a rotating dipole point source and scattered by a rigid sphere.*

The pulsating frequency of the rotating dipole point source is $f_0 = 160$ Hz. The component of the dipole source strength expressed in the cylindrical coordinate system is $\int_{f=0} L_R dS = \int_{f=0} L_\phi dS = \int_{f=0} L_Z dS = \cos(2\pi f_0 \tau)$ N. The other parameters are the same as those given in test case 1.

***Test Case 3**: Isom thickness noise radiated from a fictitious rotor and scattered by a cylinder with a finite length.*

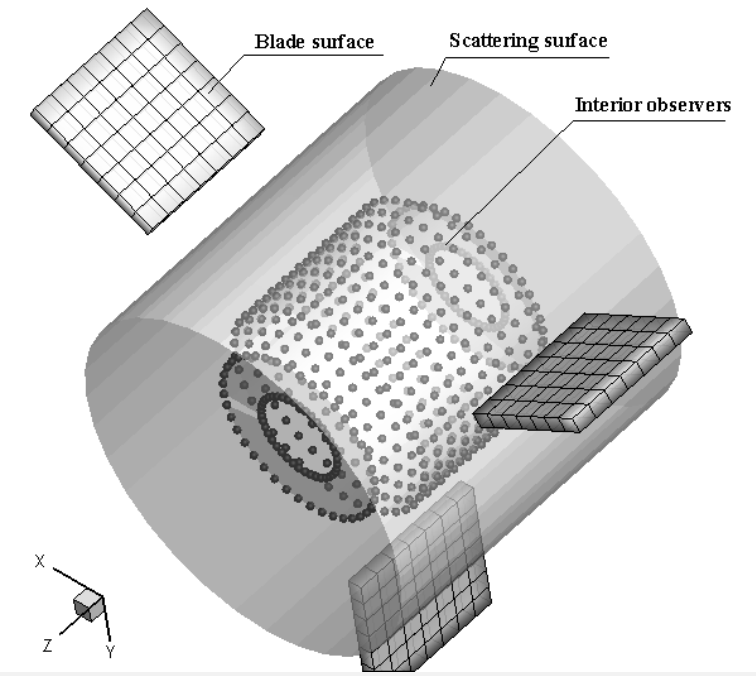

Fig. 1 Schematic of rotating blades, scattering cylinder and fictitious interior observers

Fig. 1 shows a generic rotor consisting of three equally spaced blades and a rigid scattering cylinder with a finite length. The radius and length of the scattering cylinder are 0.25m and 0.5m, respectively. The axis of the cylinder is in line with the *z* axis, and the center of the cylinder is at the origin of the coordinate system. The blade is a rectangular plate, with a chord length of 0.2m, a span of 0.2m and a thickness of 0.02m. The tip radius of the rotating blades is 0.5m, and the centerline of the rectangular plate is in the *xy* plane. The blades rotate around the Z axis with a rotational frequency f_r =60Hz, corresponding to the blade tip Mach number of $M = 0.54$. The sketch of

this test case can also be found in reference [17], and details on the property of the Isom thickness noise can be found in reference [41].

***Test Case 4**: Isom thickness noise radiated from a realistic rotor and scattered by a hub*

Thickness noise radiated from realistic rotating blades and scattered by a hub is analyzed. A schematic of the realistic rotor and the hub is shown in Fig. 2. This test case aims to analyze effects of two parameters, the hub-to-tip ratio r_h/r_t and the rotating frequency f_r, on the scattering of the rotor noise. In all the configurations, the rotating blades have the same airfoil shape, the number of rotating blades is 5, the blades tip radius is $r_t = 0.25$m, which is kept constant, and the hub length is 0.15m. Three hub radii, $r_h = 0.05$m, 0.1m and 0.15m, respectively, are tested, corresponding to the hub-to-tip ratio r_h/r_t of 20%, 40% and 60%. The rotating frequency is $f_r = 100$Hz and 150Hz, respectively, corresponding to the tip Mach number of rotating blades of 0.46 and 0.69.

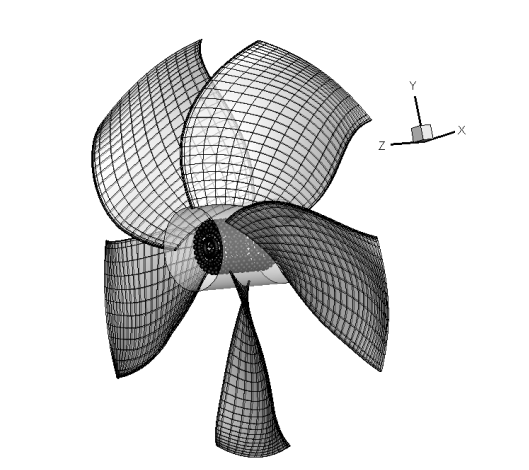

Fig. 2 Schematic of the realistic rotating blades and a hub

In all the numerical cases, the speed of sound is $c_0 = 340$ m/s and the density of the unperturbed fluid is $\rho_0 = 1.2$ kg/m^3. Sound radiates from rotating sources and propagates in quiescent fluid, without considering the effect of moving medium on acoustic propagation. In order to compute the directivity pattern in the *xz* plane, the acoustic pressure received by 61 observers is computed. The observers are equally distributed on a semi-circle ($\theta_x \in [0, \pi]$) of the radius $r_x = 2$ m, with its center at the origin of the coordinate system.

Test cases 1 and 2 are selected because analytical solutions are available [17] for comparison to validate the developed NFM. Test case 3 is a simplified model of a rotor noise scattered by a shaft. There is no analytical

solution for test case 3, but the results obtained from the ESM and the NFM will be compared with each other. Test case 4 aims to study effects of two parameters, the hub-to-tip ratio and the rotating frequency, on the rotor noise scattered by the hub. Since tonal noise is radiated from a rotating source with a monochromatic pulsating frequency, here we only compute the noise component at the first harmonic (m=1). As this paper is only for validating the developed method although noise at higher harmonics could be calculated with the same process.

B. Computational accuracy

In test cases 1 and 2, the scattering sphere is divided into 648 elements, and the coordinates of the collocation points at the center of each element are given in Cartesian coordinate system as

$$\begin{cases} x_{l,n} = \mathrm{Sin}[\dfrac{\pi}{19}l]\mathrm{Cos}[\dfrac{2\pi}{36}n]\ \mathrm{m} \\ y_{l,n} = \mathrm{Sin}[\dfrac{\pi}{19}l]\mathrm{Sin}[\dfrac{2\pi}{36}n]\ \mathrm{m}\ (l=1,2,...18; n=1,2,...36) \\ z_{l,n} = \mathrm{Cos}[\dfrac{\pi}{19}l]\ \mathrm{m} \end{cases} \tag{11}$$

It can be easily found that the collocation points are uniformly located on 18 circles, where 36 points are uniformly distributed on each circle. In the ESM and the NFM, a SR is predefined to locate the equivalent sources and the fictitious observers. Note that, in OLM1 of the NFM, the acoustic pressure received by each fictitious observer is computed by numerical integral. However, in OLM2 of the NFM, only the acoustic pressure received by one observer on each circle is required to perform a numerical integral, the acoustic pressure received by other observers on the same circle is calculated from Eq. (9) without numerical integral. Owing to this treatment, it is expectable that OLM2 will greatly reduce the computational time and a comparison of these two methods will be given in Section III.C.

Fig. 3 and Fig. 4 display the directivity patterns for test cases 1 and 2, respectively, where the SR is set to be 0.5. The numerical results obtained from both the ESM and the NFM are in good agreement with the analytical solutions. Moreover, a parametric study is carried out to analyze the effect of the SR on the computational accuracy. A relative root-mean-square (RMS) error has been defined to characterize the deviation of the numerical result from the analytical solution

$$\varepsilon = \frac{1}{\max\left|\tilde{p}'_A(\phi_{\mathbf{x},l})\right|}\sqrt{\frac{\sum_{l=1}^{N_O}\left|\tilde{p}'_N(\phi_{\mathbf{x},l})-\tilde{p}'_A(\phi_{\mathbf{x},l})\right|^2}{N_O}} \tag{12}$$

where subscript N represents the numerical result from ESM or the NFM, and subscript A represents the analytical solution; subscript l means the lth observer, N_O is the number of observers.

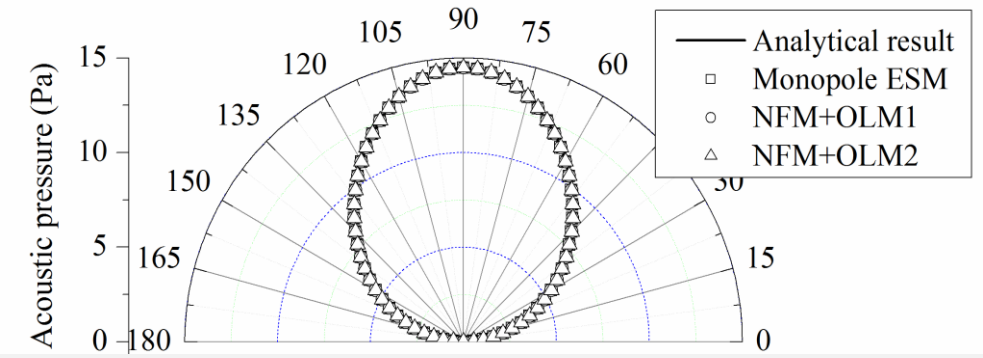

Fig. 3 Directivity pattern of overall noise for rotating monopole point source

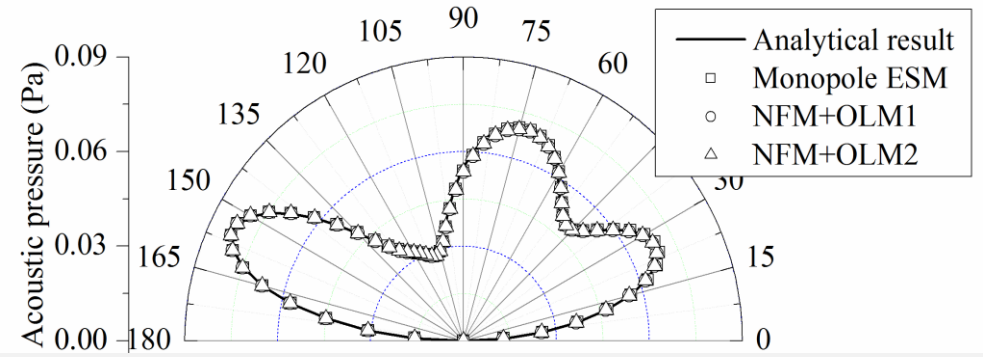

Fig. 4 Directivity pattern of overall noise for rotating dipole point source

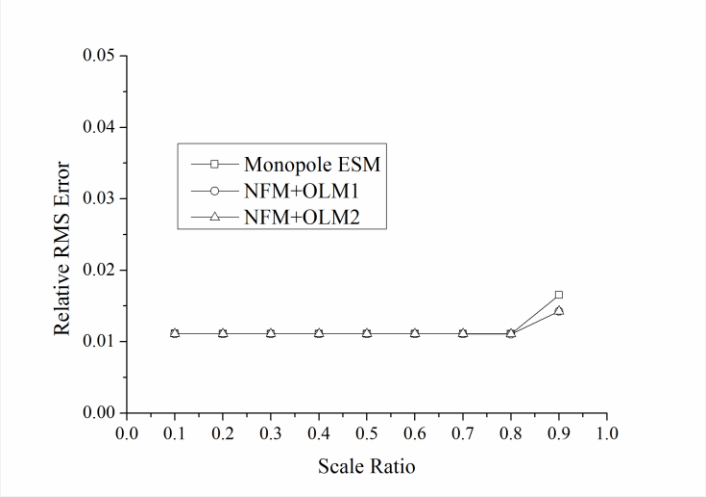

Fig. 5 The relative RMS error for the case of rotating monopole point source

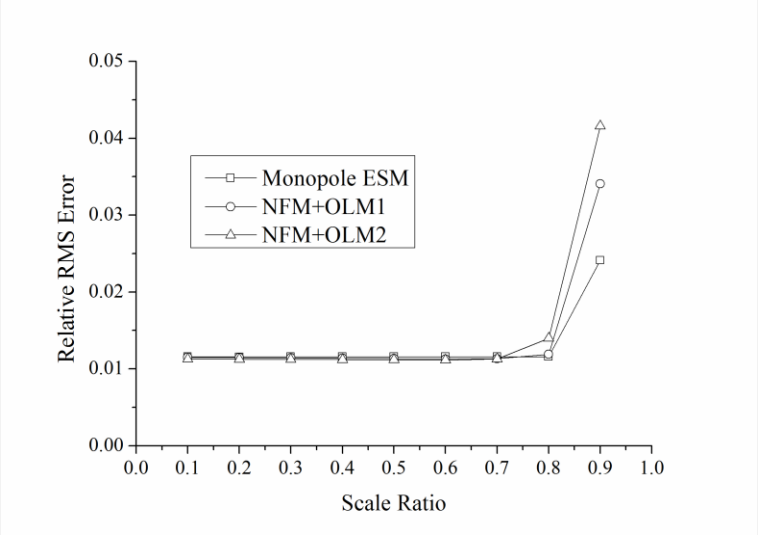

Fig. 6 The relative RMS error for the case of rotating dipole point source

Fig. 5 and Fig. 6 show the relative RMS errors for the ESM and the NFM. The errors for all three methods stay around 1.2% for SR ranging between 0.1 and 0.8. For SR=0.9, the relative errors increase but are still lower than 2% for the monopole case, and 5% for the dipole case. This result validates that both the numerical methods provide an enough accuracy to predict scattered noise from the rotating source.

As show in Fig. 1, all six surfaces of each rotating blade are discretized in test case 3. The number of elements along the directions of blade chord, span and thickness are 7, 7 and 1, respectively. It has been demonstrated [17] that this mesh discretization scheme on the rotating blades is fine enough to guarantee accurate computation of the thickness noise and steady loading noise by conducting the consistency test of the Isom property [41]. In this paper, the scattering cylindrical surface is divided into 560 elements, where all the collocation points on the elements are located on 14 circles. The coordinate of the collocation points located on the lateral surface of the cylinder is expressed as

$$\begin{cases} x_{l,n} = 0.25\mathrm{Cos}[\dfrac{2\pi}{40}n]\ \mathrm{m} \\ y_{l,n} = 0.25\mathrm{Sin}[\dfrac{2\pi}{40}n]\ \mathrm{m} \quad (l=1,2,...10; n=1,2,...40) \\ z_{l,n} = -0.2+0.04(l-1)\ \mathrm{m} \end{cases} \tag{13}$$

The coordinate of the collocation points located on the two end surfaces is expressed as

$$\begin{cases} x_{l,n} = 0.1l\mathrm{Cos}[\dfrac{2\pi}{40}n]\ \mathrm{m} \\ y_{l,n} = 0.1l\mathrm{Sin}[\dfrac{2\pi}{40}n]\ \mathrm{m} \quad (l=1,2;n=1,2,...40) \\ z_{l,n} = \pm 0.25\ \mathrm{m} \end{cases} \tag{14}$$

In both the ESM and the NFM, the SR is set to 0.6. The number of the equivalent point sources is one third of the number of the elements on the scattering surface, whereas the number of the fictitious interior observers is equal to the number of the elements on the scattering surface. Fig. 7 compares the numerical result obtained from the ESM with that obtained from the NFM. The directivity pattern for all the numerical results is in consistent with each other, but there is a small deviation between the present numerical results with the results presented in reference [17]. This small deviation is due to the different mesh discretization of the scattering cylindrical surface.

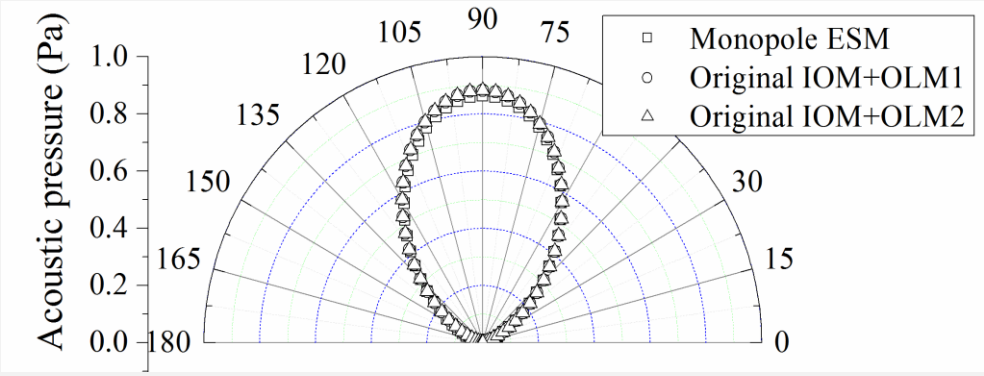

Fig. 7 Directivity pattern of overall noise for rotating blades

C. Computational efficiency

All the computational codes are executed on a personal computer with Intel Core i7-620M CPU and 4G RAM. Table 2 displays the computational time for the case of the monopole point source with SR=0.5. In the ESM, the computational time for constructing the matrix **A** is almost the same as that for constructing the vector **b.** Moreover, the computational time for constructing the matrix **A** in the NFM is also similar to that in the ESM, but the computational time for constructing the vector **b** in the NFM is much less than that in the ESM. In order to construct the vector **b**, the incident acoustic pressure is computed in the NFM while all three components of the incident acoustic velocity need to be computed in the ESM, thus the NFM is more efficient than the ESM. Moreover, when OLM2 and Eq. (9) are employed to locate the fictitious interior observers and to fast compute the incident acoustic

pressure, the computational time for constructing the vector **b** is much less than that for constructing the matrix **A**. A similar conclusion can be drawn from the case of the dipole point source, as shown in Table 3.

Table 2 Computational time for the case of monopole point source with SR=0.5

	Construction of **A**	Construction of **b**	Solution of $\mathbf{A}\boldsymbol{\xi}=\mathbf{b}$	Total time
ESM	26.7s	25.7s	5.3s	57.7s
NFM+OLM1	24.5s	5.6s	9.4s	39.4s
NFM+OLM2	24.5s	0.1s	5.4s	30.0s

Table 3 Computational time for the case of dipole point source with SR=0.5

	Construction of **A**	Construction of **b**	Solution of $\mathbf{A}\boldsymbol{\xi}=\mathbf{b}$	Total time
ESM	22.3s	42.0s	7.1s	71.4s
NFM+OLM1	23.2s	10.6s	8.1s	41.9s
NFM+OLM2	23.2s	0.7s	5.1s	29.0s

It should be noted that, in test cases 1 and 2, the incident noise is radiated from a single point source. For a real rotor configuration, computation of the incident noise radiated from numerous surface elements on the rotating blades will be more computationally demanding, the proposed method in this paper will be more beneficial to reduce the computational time.

Table 4 Computational time for the case of rotating blades with SR=0.6

	Construction of **A**	Construction of **b**	Solution of $\mathbf{A}\boldsymbol{\xi}=\mathbf{b}$	Total time
ESM	7.5s	5559.6s	0.9s	5568.0s
NFM+OLM1	7.4s	981.8s	5.3s	994.5s
NFM+OLM2	7.4s	24.1s	3.6s	35.1s

Table 4 displays the computational time of test case 3. Since the incident noise is radiated from many compact elements on the rotating blades, constructing the vector **b** costs much more time than constructing the matrix **A** if the incident noise is numerically computed for each source-observer pair one by one, as is used for the ESM and the NFM combined with OLM1. However, when the NFM is combined with OLM2, the computational time is greatly reduced, validating its significant advantage in the computational efficiency.

Moreover, in test cases 1 and 2, the number of the equivalent sources and the fictitious observers is the same as that of the surface elements. Actually, the number of the equivalent sources can be less than that of the surface elements, thus it can reduce the computational time of constructing the matrix **A** and solving the equation system in the ESM. However, constructing the vector **b** is independent of the number of equivalent sources, thus fewer number of equivalent sources has little effect on the total computational time of the ESM.

D. Parametric study of a rotor noise scattered by a hub

As shown in Fig. 2, each blade surface is discretized into 1050 compact elements, 420 interior fictitious observers are evenly located on a cylindrical surface inside the shaft with SR=0.2, which is discretized to 14 circles for numerical representation. The singular value decomposition method [11] is used to solve the linear equation. Fig. 8-Fig. 11 present the computed directivity patterns for the rotor configurations with three hub-tip ratios and at two rotating frequencies.

Firstly, we analyze effects of the above two parameters on the radiation of the thickness noise in free space. The blade span and the surface area decrease with the increase of the hub-tip ratio, thus the thickness noise radiated into the free space also deceases with the increase of the hub-tip ratio, as shown in Fig. 8-Fig. 10. Comparing Fig. 9 with Fig. 11, it is obvious that the thickness noise increases with the rotating frequency.

Secondly, we investigate the effect of the above two parameters on the hub scattering. As shown in Fig. 8, the scattered component cannot be observed, because it is much smaller than the component radiated from the rotating blades. Therefore, the hub scattering can be ignorable if the hub-tip ratio is very small. However, the effect of the hub scattering is more evident with the increase of the hub-tip ratio, as shown in Fig. 9 and Fig. 10. This conclusion is consistent with the findings of Glegg [42], who analytically accounted for the hub scattering by using a tailored Green's function of a rigid cylinder. Fig. 10 also indicates that at large hub-tip ratios the directivity pattern changes due to a greater influence of the two end surfaces of the hub on sound scattering. The acoustic pressures received by observers located near the two end surfaces of the hub are different from each other because the normal component

of the rotating velocity on the blade surface, which is directly related to the strength of the steady thickness source, depends on the local blade stagger angle. This phenomenon can neither be observed in [42] because the length of the cylinder is assumed to be infinite, nor in test case 3 because the cylinder and the three rectangular plates are symmetric and aligned with the axis of the cylindrical hub.

Now, we analyze the rotating frequency on the hub scattering by comparing the computational results illustrated in Fig. 9 and Fig. 11. The hub scattering becomes negligible with the increase of the rotating frequency (sound wavenumber). In summary, for noise radiated from the steady thickness source on the rotating blade surfaces, the effect of the hub scattering may become significant for a large hub-tip ratio and a low sound wavenumber, and this conclusion is absolutely consistent with that drawn in [42].

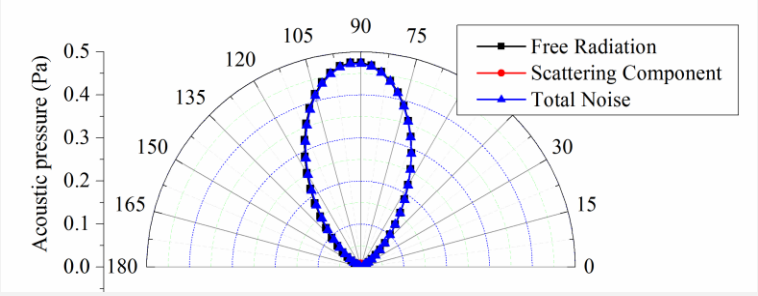

Fig. 8 Directivity pattern of rotor noise: r_h/r_t =20% and f_r = 100Hz

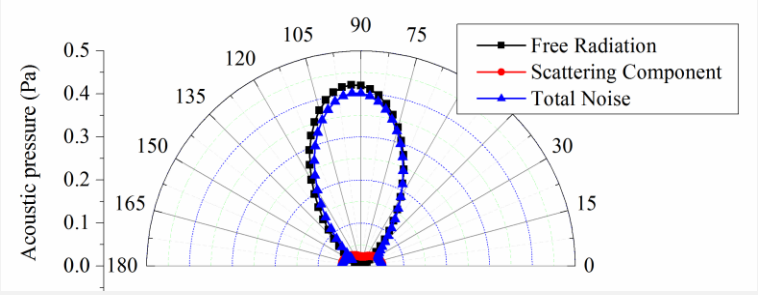

Fig. 9 Directivity pattern of rotor noise: r_h/r_t =40% and f_r = 100Hz

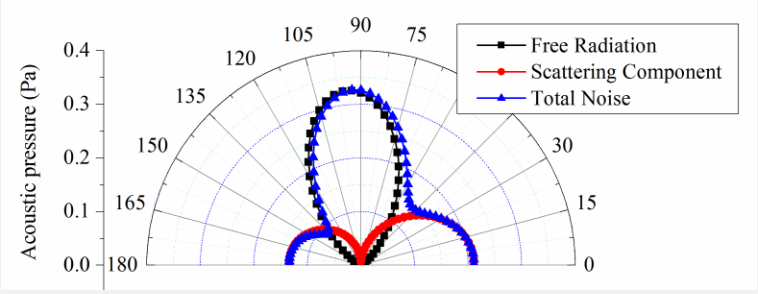

Fig. 10 Directivity pattern of rotor noise: r_h/r_t =60% and f_r = 100Hz

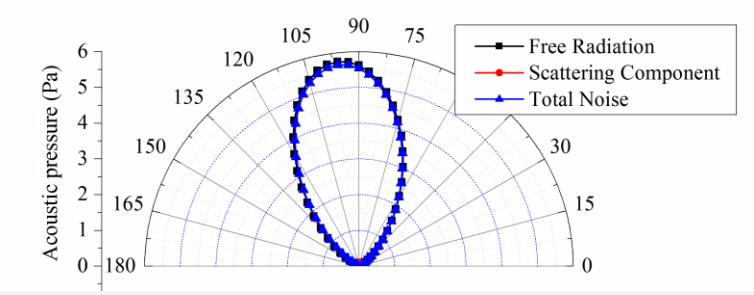

Fig. 11 Directivity pattern of rotor noise: r_h/r_t =40% and f_r = 150Hz

IV. Conclusions

This paper proposes a new method, by combining the frequency-domain numerical method with the NFM, for predicting the noise radiated from rotating sources and scattered by an axisymmetric body. Four test cases are carried out to validate the computational accuracy of the developed method. Moreover, the paper emphasizes the advantage of the developed method in improving the computational efficiency owing to the following two reasons. The first is that it avoids computing the incident acoustic velocity or the acoustic pressure gradient that are required in the ESM and the BEM. The second is a fast computation of the incident acoustic pressure radiated from the rotating sources by employing an advanced method to locate fictitious interior observers. Parametric studies of a realistic rotor configuration indicate that the effect of the hub scattering becomes more evident at large hub-tip ratios and small sound wavenumbers (low frequencies). The present paper has not considered the effect of moving medium on acoustic propagation, and this research topic will be reported in future.

Acknowledgments

The research has been supported by the National Natural Science Foundation of China (No. 51476123). Partial research is carried out under the joint support of the National Natural Science Foundation of China (No. 51511130075) and Newton Fund (No. IE141516). Yijun Mao acknowledges China Scholarship Council for supporting his academic visit in University of Southampton. The authors acknowledge the anonymous reviewers for their valuable comments to improve the quality of the paper.

References

[1] Keller, J. B., and Givoli, D. "Exact Non-Reflecting Boundary Conditions," *Journal of Computational Physics* Vol. 82, No. 1, 1989, pp. 172-192.
doi: 10.1016/0021-9991(89)90041-7

[2] Berenger, J. P. "A Perfectly Matched Layer for the Absorption of Electromagnetic Waves," *Journal of computational physics* Vol. 114, No. 2, 1994, pp. 185-200.
doi:10.1006/jcph.1994.1159

[3] Astley, R. "Infinite Elements for Wave Problems: A Review of Current Formulations and An Assessment of Accuracy," *International Journal for Numerical Methods in Engineering* Vol. 49, No. 7, 2000, pp. 951-976.
doi:10.1002/1097-0207(20001110)49:7<951::AID-NME989>3.0.CO;2-T

[4] Astley, R., Sugimoto, R., and Mustafi, P. "Computational Aero-Acoustics for Fan Duct Propagation and Radiation. Current Status and Application to Turbofan Liner Optimisation," *Journal of Sound and Vibration* Vol. 330, No. 16, 2011, pp. 3832-3845.
doi:10.1016/j.jsv.2011.03.022

[5] Schenck, H. A. "Improved Integral Formulation for Acoustic Radiation Problems," *The Journal of the Acoustical Society of America* Vol. 44, No. 1, 1968, pp. 41-58.
doi:10.1121/1.1911085

[6] Burton, A., and Miller, G. "The Application of Integral Equation Methods to the Numerical Solution of Some Exterior Boundary-Value Problems," *Proceedings of the Royal Society of London A: Mathematical, Physical and Engineering Sciences*. Vol. 323, 1971, pp. 201-210.
doi: 10.1098/rspa.1971.0097

[7] Yan, Z. Y., Hung, K. C., and Zheng, H. "Solving the Hypersingular Boundary Integral Equation in Three-Dimensional Acoustics Using a Regularization Relationship," *The Journal of the Acoustical Society of America* Vol. 113, No. 5, 2003, pp. 2674-2683.
doi: 10.1121/1.1560164

[8] Tadeu, A., and António, J. "3D Acoustic Wave Simulation Using BEM Formulations: Closed Form Integration of Singular and Hypersingular Integrals," *Engineering Analysis with Boundary Elements* Vol. 36, No. 9, 2012, pp. 1389-1396.
doi:10.1016/j.enganabound.2012.03.011

[9] Mark, D., and Ana, T. "Aeroacoustic Scattering via the Equivalent Source Method," AIAA Paper 2004-2937, 2004.
doi: 10.2514/6.2004-2937

[10] Lee, S. K., Brentner, K. S., and Morris, P. J. "Acoustic Scattering in the Time Domain Using an Equivalent Source Method," *AIAA Journal* Vol. 48, No. 12, 2010, pp. 2772-2780.
doi: 10.2514/1.45132

[11] Lee, S. K., Brentner, K. S., and Morris, P. J. "Assessment of Time-Domain Equivalent Source Method for Acoustic Scattering," *AIAA Journal* Vol. 49, No. 9, 2011, pp. 1897-1906.
doi: 10.2514/1.J050736

[12] Ghorbaniasl, G., Carley, M., and Lacor, C. "Acoustic Velocity Formulation for Sources in Arbitrary Motion," *AIAA Journal* Vol. 51, No. 3, 2013, pp. 632-642.
doi: 10.2514/1.J051958

[13] Mao, Y. J., Zhang, Q. L., Xu, C., and Qi, D. T. "Two Types of Frequency-Domain Acoustic-Velocity Formulations for Rotating Thickness and Loading Sources," *AIAA Journal* Vol. 53, No. 3, 2015, pp. 713-722.
doi: 10.2514/1.j053230

[14] Lee, S. K., Brentner, K. S., Farassat, F., and Morris, P. J. "Analytic Formulation and Numerical Implementation of an Acoustic Pressure Gradient Prediction," *Journal of Sound and Vibration* Vol. 319, No. 3-5, 2009, pp. 1200-1221.
doi:10.1016/j.jsv.2008.06.028

[15] Mao, Y. J., Xu, C., and Qi, D. T. "Computation of Instantaneous and Time-Averaged Active Acoustic Intensity Field around Rotating Source," *Journal of Sound and Vibration* Vol. 337, 2015, pp. 95-115.
doi: 10.1016/j.jsv.2014.10.023

[16] Mao, Y. J., Cai, J. C., Gu, Y. Y., and Qi, D. T. "Direct Evaluation of Acoustic Intensity Vector Field around Impedance Scattering Body," *AIAA Journal* Vol. 53, No. 5, 2015, pp. 1362-1371.
doi: 10.2514/1.J053431

[17] Mao, Y. J., Gu, Y. Y., and Xu, C. "Validation of Frequency-Domain Method to Compute Noise Radiated from Rotating Source and Scattered by Surface," *AIAA Journal*, Vol. 54, No.4, 2016, pp. 1188-1197.
doi: 10.2514/1.J053674

[18] Waterman, P. "Matrix Formulation of Electromagnetic Scattering," *Proceedings of the IEEE* Vol. 53, No. 8, 1965, pp. 805-812.
doi: 10.1109/PROC.1965.4058

[19] Waterman, P. C. "New Formulation of Acoustic Scattering," *The Journal of the Acoustical Society of America* Vol. 45, No. 6, 1969, pp. 1417-1429.
doi:10.1121/1.1911619

[20] Mishchenko, M. I., Travis, L. D., and Mackowski, D. W. "T-matrix Computations of Light Scattering by Nonspherical Particles: A Review," *Journal of Quantitative Spectroscopy and Radiative Transfer* Vol. 55, No. 5, 1996, pp. 535-575.
doi: 10.1016/0022-4073(96)00002-7

[21] Cunefare, K. A., Koopmann, G., and Brod, K. "A Boundary Element Method for Acoustic Radiation Valid for All Wavenumbers," *The Journal of the Acoustical Society of America* Vol. 85, No. 1, 1989, pp. 39-48.
doi: 10.1121/1.397691

[22] Martin, P. A. "On the Null-Field Equations for the Exterior Problems of Acoustics," *Quarterly Journal of Mechanics and Applied Mathematics* Vol. 33, No. Nov, 1980, pp. 385-396.
doi: 10.1093/qjmam/33.4.385

[23] Martin, P. A. "Acoustic Scattering and Radiation Problems, and the Null-Field Method," *Wave Motion* Vol. 4, No. 4, 1982, pp. 391-408.
doi: 10.1016/0165-2125(82)90007-5

[24] Darve, E. "The fast Multipole Method: Numerical Implementation," *Journal of Computational Physics* Vol. 160, No. 1, 2000, pp. 195-240.
doi:10.1006/jcph.2000.6451

[25] Kingan, M. J., and Self, R. H. "Open Rotor Tone Scattering," *Journal of Sound and Vibration* Vol. 331, No. 8, 2012, pp. 1806-1828.
doi: 10.1016/j.jsv.2011.12.001

[26] Kingan, M. J., and Sureshkumar, P. "Open Rotor Centrebody Scattering," *Journal of Sound and Vibration* Vol. 333, No. 2, 2012, pp. 418-433.
doi: 10.1016/j.jsv.2013.08.010

[27] Dunn, M. H., Tweed, J., and Farassat, F. "The Application of a Boundary Integral Equation Method to the prediction of ducted fan engine noise," *Journal of Sound and Vibration* Vol. 227, No. 5, 1999, pp. 1019-1048.
doi: 10.1006/jsvi.1999.2394

[28] Hu, B. B., OuYang, H., Wu, Y. D., Jin, G. Y., Qiang, X. Q., and Du, Z. H. "Numerical Prediction of the Interaction Noise Radiated from an Axial Fan," *Applied Acoustics* Vol. 74, No. 4, 2013, pp. 544-552.
doi: 10.1016/j.apacoust.2012.09.009

[29] Tang, H. T., Qi, D. T., and Mao, Y. J. "Analysis on the Frequency-Domain Numerical Method to Compute the Noise Radiated from Rotating Sources," *Journal of Sound and Vibration* Vol. 332, No. 23, 2013, pp. 6093-6103.
doi: 10.1016/j.jsv.2013.06.020

[30] Mao, Y. J., and Xu, C. "Accelerated method for Predicting Acoustic Far Field and Acoustic Power of Rotating Source," *AIAA Journal*, Vol. 54, No.2, 2016, pp. 603-615.
doi: 10.2514/1.J054425

[31] Farassat, F. "Derivation of Formulations 1 and 1A of Farassat." NASA TM 2007-214853, 2007.

[32] Mao, Y. J., Gu, Y. Y., Qi, D. T., and Tang, H. T. "An Exact Frequency-Domain Solution of the Sound Radiated from the Rotating Dipole Point Source," *Journal of the Acoustical Society of America* Vol. 132, No. 3, 2012, pp. 1294-1302.
doi: 10.1121/1.4742972

[33] Mao, Y. J., Xu, C., Qi, D. T., and Tang, H. T. "Series Expansion Solution for Sound Radiation from Rotating Quadrupole Point Source," *AIAA Journal* Vol. 52, No. 5, 2014, pp. 1086-1095.
doi: 10.2514/1.j052706

[34] Mao, Y. J., and Qi, D. T. "Computation of Rotating Blade Noise Scattered by a Centrifugal Volute," *Proceedings of the Institution of Mechanical Engineers, Part A, Journal of Power and Energy* Vol. 223, No. 8, 2009, pp. 965-972.
doi: 10.1243/09576509jpe794

[35] Gounot, Y. J., and Musafir, R. E. "On Appropriate Equivalent Monopole Sets for Rigid Body Scattering Problems," *The Journal of the Acoustical Society of America* Vol. 122, No. 6, 2007, pp. 3195-3205.
doi: 10.1121/1.2799504

[36] Ochmann, M. "The Full-Field Equations for Acoustic Radiation and Scattering," *Journal of the Acoustical Society of America* Vol. 105, No. 5, 1999, pp. 2574-2584.
doi: 10.1121/1.426873

[37] Ochmann, M. "The Complex Equivalent Source Method for Sound Propagation over an Impedance Plane," *The Journal of the Acoustical Society of America* Vol. 116, No. 6, 2004, pp. 3304-3311.
doi:10.1121/1.1819504

[38] Hou, Y., Zhang, X., and Angland, D. "A Complex Equivalent Source Method for Scattering Effect of Aircraft Noise," AIAA Paper 2014-3302, 2014.
doi:10.2514/6.2014-3302

[39] Cheng, B. F., Brentner, K. S., and Morris, P. J. "Validation of a Time-Domain Equivalent Source Method for Acoustic Scattering by an Oblate Spheroid," AIAA Paper 2013-0759, 2013.
doi:10.2514/6.2013-759

[40] Swift, S., Blaisdell, G., and Lyrintzis, A. "An Efficient Time-Domain Equivalent Source Method for Acoustic Scattering," *International Journal of Aeroacoustics* Vol. 14, No. 1, 2015, pp. 133-160.
doi: 10.1260/1475-472X.14.1-2.133

[41] Farassat, F., and Nystrom, P. A. "Isoms Thickness Noise Formula for Rotating Blades with Finite Thickness at the Tip," *Journal of Sound and Vibration* Vol. 72, No. 4, 1980, pp. 550-553.
doi: 10.1016/0022-460x(80)90366-1

[42] Glegg, S A L. "Effect of Centerbody Scattering on Propeller Noise," *AIAA Journal* Vol. 29, No. 4, 1991, pp. 572-576.
doi: 10.2514/3.10622